Article:
Li, F, Li, K orcid.org/0000-0001-6657-0522, Peng, C et al. (1 more author) (2023) Dynamic event-triggered fuzzy control of DC microgrids under FDI attacks and imperfect premise matching. International Journal of Electrical Power and Energy Systems, 147. 108890. ISSN 0142-0615

https://doi.org/10.1016/j.ijepes.2022.108890

Dynamic event-triggered fuzzy control of DC microgrids under FDI attacks and imperfect premise matching

Fuqiang Li[a,b,*], Kang Li[b], Chen Peng[c], Lisai Gao[c]

[a] *College of Sciences, Henan Agricultural University, Zhengzhou, 450002, China*
[b] *School of Electronic and Electrical Engineering, University of Leeds, Leeds, LS29JT, UK*
[c] *Shanghai Key Laboratory of Power Station Automation Technology, School of Mechatronics Engineering and Automation, Shanghai University, Shanghai, 200444, China*

Abstract

This paper investigates the T-S fuzzy control of DC microgrids subject to false data injection (FDI) attacks, premise mismatching, and network delays using a dynamic event-triggered mechanism (ETM). Unlike the static ETMs using the fixed triggering parameters, by adaptively adjusting the triggering parameters, the proposed novel discrete-time dynamic ETM can more effectively reduce excessive usage of communication resources, and the Zeno behavior is also avoided naturally. Then, a novel T-S fuzzy closed-loop system model is built, which considers the FDI attacks, dynamic ETM, delays and premise mismatching all in one unified framework. Mean-square exponential stability criteria are derived, which establish the relationship between system performance and the contributing factors. Further, unlike the two-step emulation based method, the proposed co-design method can design the injection current controller and the dynamic ETM in one step, which offers a convenient framework for the tradeoffs between control and communication performances. Both simulation and experimental results confirm the effectiveness of the proposed methods, achieving 27.5% savings of communication resources while effectively stabilizing the DC microgrid even under the situation that 13.5% of the transmitted data are tampered by the FDI attacks.

Keywords: DC microgrid; dynamic event-triggered mechanism; false data injection attacks; T-S fuzzy control; mean-square exponential stability

*Corresponding author. E-mail address: lifuqiang@henau.edu.cn (Fuqiang Li)

1. Introduction

To achieve the decarbonization objective of energy systems, it is imperative to develop greener electrification systems, which prompts a massive growth of renewable generation technologies such as the solar photovoltaics (PV) technology [1]. By seamlessly integrating these distributed energy resources into the electric grid, the microgrid brings a suite of operational, technical and economic benefits such as optimized energy economics and increased reliability. Compared with AC microgrids, DC microgrids do not have the issues of synchronization, reactive power flow, harmonics, etc., while can easily interface with renewable energy resources, energy storage systems (ESSs) and electric loads due to their natural DC behavior [2]. Thus, DC microgrids have been widely used in renewable energy systems, electric vehicles/aircrafts/ships, remote households, etc.

In a DC microgrid, tightly regulated power electronic loads are likely to draw constant power, which can be seen as constant power loads (CPLs). However, the negative impedance feature of the CPLs decreases the system damping and may even result in instability [3]. To handle the CPL-induced issues, the passive damping method has been proposed by adding passive components such as physical resistor. Although the passive damping method is simple and effective, it is often costly and hard to implement due to physical constraints. As an energy efficient alternative, the active damping strategy has been presented by designing virtual impedances in the control loops to mimic the same behavior of physical impedances. However, due to the usage of small signal models, the active damping method can only guarantee small signal stability near the equilibrium point [4]. To ensure a large signal stability, advanced control strategy should be deployed. On the other hand, the T-S fuzzy method works well in modelling nonlinear systems [5], and can use simple linear controllers to achieve the semi-global stability. However, it has not drawn enough attention to apply the T-S fuzzy method to the DC microgrid, which is our first motivation.

To establish the hierarchical control structure in a DC microgrid, it is necessary to establish communication networks to share data among measurement devices and controller nodes, which makes microgrids vulnerable to cyber attacks. These attacks can be mainly classified into FDI attacks and denial of service (DoS) attacks. FDI attacks intend to tamper the orig-

inal signals by injecting false data, while DoS attacks attempt to block the communication network [6]. Since adversaries often intentionally design the injecting attacks to bypass the conventional surveillance and security techniques, FDI attacks are more stealthy and destructive, which motivates this study.

Recently, some researches have been conducted on mitigating the impacts of FDI attacks in DC microgrid. For instance, to address the impacts from the FDI attacks which modify the onboard current and voltage sensors in a four converter-based DC microgrid, the work in [7] proposes an adaptive state observer based attack detection and correction mechanism. For the FDI attacks in DC microgrid formed by parallel DC-DC converters, the work in [8] presents an attack detection and mitigation method using artificial neural networks and model predictive control. While the aforementioned studies focus on the attack detection methods, some other works investigate the security control of DC microgrids. For instance, for the FDI attacks affecting the current sensors of distributed generation units (DGUs) in DC microgrids, [9] proposes an adaptive observer to reconstruct the attacks and necessary stability conditions are further derived. For the FDI attacks affecting both the proportional current and the average voltage, the work in [10] presents a resilient control methodology, including a state limitation method and an integrated distributed control strategy. By modeling the distributed energy resources as multi-agent systems, for FDI attacks affecting the leader and follower nodes, [11] proposes a secondary control method based on a distributed sliding mode observer. Although many useful results have been presented in these researches, the limited network bandwidth is often ignored.

The constrained network bandwidth often jeopardizes the performance of DC microgrids in forms of delays, dropouts, congestion, etc. Since DC microgrids traditionally adopt the periodic control strategy, to assure system stability under the worst conditions, sampling period is often set small. However, the high sampling frequency tends to cause network congestion. Besides, when system has been in the steady state without disturbances, it is often unnecessary to still frequently execute control tasks. Fortunately, an alternative solution to the periodic control, namely the event-triggered control (ETC) strategy, has been proposed [12]. By executing control tasks only when system needs attention, the ETC strategy can guarantee system performance while saving communication resources. Recently, the ETC method has been introduced in DC microgrids. For instance, using the triggering condition derived from Lyapunov function to reduce communication cost,

the work in [13] proposes a hierarchical distributed event-triggered consensus algorithm for the ESSs in DC microgrid clusters. Using output current information to design the triggering condition, [14] presents a voltage observer based distributed ETC algorithm for accurate voltage profile regulation and load current sharing in DC microgrids. Using control signals to design the triggering condition with a constant triggering threshold, the work in [15] presents a distributed secondary ETC strategy for DC microgrids. Using both system states and a constant to design the triggering threshold, [16] studies the consensus-based secondary ETC for the DGUs in DC microgrids. Although some interesting results have been achieved, there still exist the following limitations. First, for the continuous time ETM, it is not easy to exclude the Zeno behavior. Second, threshold parameters of the ETM are often fixed during system operation, which is conservative due to the ignorance of system dynamics. Third, the existing ETMs may not be directly applicable to the attacked DC microgrids. Thus, considering effects of the FDI attacks, it is necessary to develop a novel Zeno-free dynamic ETC strategy for DC microgrids, which is the second motivation.

To adddress the aforementioned issues, this paper investigates the T-S fuzzy security control of DC microgrids using the dynamic ETM scheme, subject to the FDI attacks, network delays and imperfect premise matching, which has the following challenges: first, the dynamic ETM results in non-continuous data transmission and premise mismatching between the microgrid and controller, which makes it difficult to build the closed-loop model under the T-S fuzzy framework. Second, for stabilizing the microgrid under the dynamic ETM, and subject to FDI attacks, delays, premise mismatching, and CPL-induced instability issue, to establish the relationship between the controller gains and these affecting factors is a challenge. The main contributions of the paper are summarized as follows.

- Compared with the continuous-time static ETMs [14, 15, 16, 17], the proposed dynamic ETM can not only save more communication resources by adaptively adjusting its threshold parameters, but also exclude Zeno behavior naturally due to its discrete-time feature.

- Unlike the works [18, 19] which assume perfect premise matching, a more generalized fuzzy closed-loop model for the DC microgrid is established under the imperfect premise matching scheme, which provides a way to study effects of the FDI attacks, the dynamic ETM, network

delays, premise mismatching and CPL-induced instability issue all in one unified framework.

- Unlike the work [20] which uses the robust linear control method, a novel event-triggered fuzzy nonlinear control strategy is proposed, and a mean-square exponential stability criteria is presented to establish the relationship between the injection current controller and the aforementioned affecting factors. Further, a co-design method for the controller and the dynamic ETM is provided, and both the simulation and experimental results confirm that the proposed controller performs better than the robust linear controller [20] in terms of overshoot and settling time.

Notation. $Diag\{\cdot\}$ is diagonal matrix, while $col\{\cdot\}$ is column matrix. $A + A^T$ is marked by $He\{A\}$. I refers to identity matrix. $\mathbb{E}\{\cdot\}$ indicates mathematical expectation of random variables. $Max\{\cdot\}$ is the maximum function, while $min\{\cdot\}$ is the minimum function. λ_{min} indicates the minimum eigenvalue. $\mathbb{E}\{\cdot\}$ refers to the mathematical expectation of random variables. $\mathbb{R}$ is real-number set, while $\mathbb{N}$ is natural-number set. $*$ indicates a symmetric item. Euclidean norm is marked by $\|\cdot\|$.

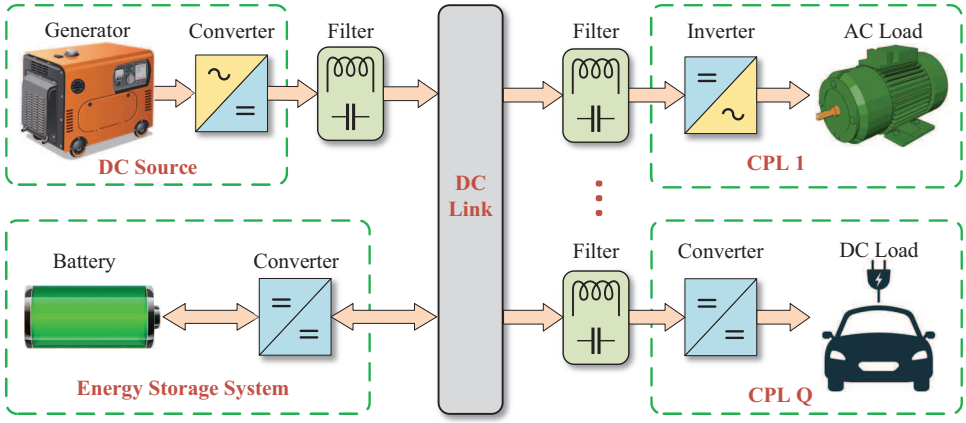

Figure 1: DC microgrid containing Q CPLs.

2. System Modelling of the DC microgrid

2.1. System description

As shown in Figure 1, a typical DC microgrid comprises a DC source, an energy storage system (ESS) and several CPLs. The constant DC source supplies the DC bus, the ESS provides the injection current, and the CPLs refer to the tightly-regulated AC or DC loads achieving constant power at the input side of their converters. Figure 2 shows the circuit of the DC microgrid, which consists of the DC source subsystem, the injection current source i_{es} and the Q CPL subsystems. The simplified circuits at the CPL side and the DC source side are shown in Figure 3.

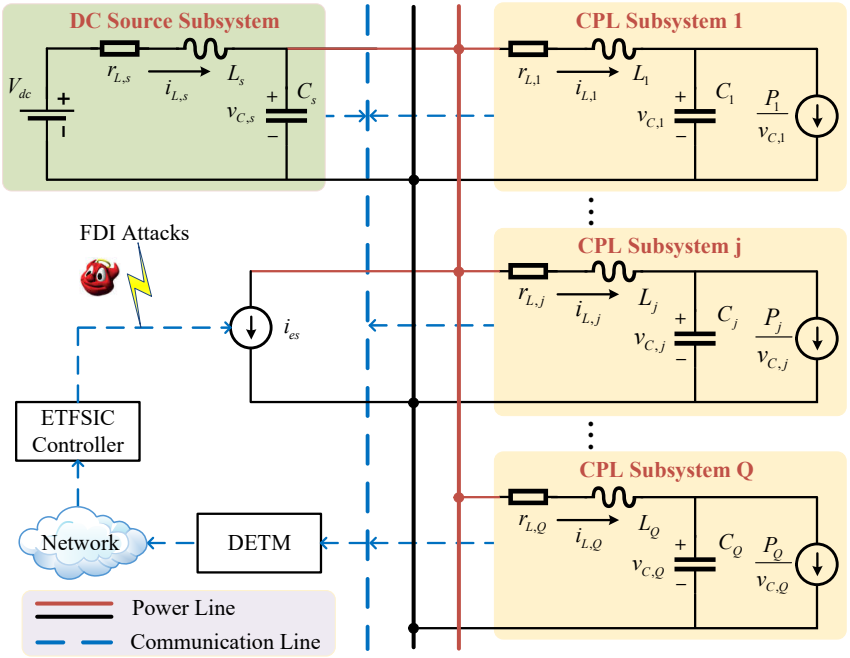

Figure 2: Circuit of the DC microgrid containing Q CPLs.

Applying the Kirchhoff circuit laws to the j_{th} CPL subsystem in Figure 3 (a) yields

$$\begin{cases} \dot{i}_{L,j} = \frac{1}{L_j} v_{C,s} - \frac{r_{L,j}}{L_j} i_{L,j} - \frac{1}{L_j} v_{C,j} \\ \dot{v}_{C,j} = \frac{1}{C_j} i_{L,j} - \frac{1}{C_j} \frac{P_j}{v_{C,j}}, \ j = 1, 2, \ldots, Q \end{cases} \tag{1}$$

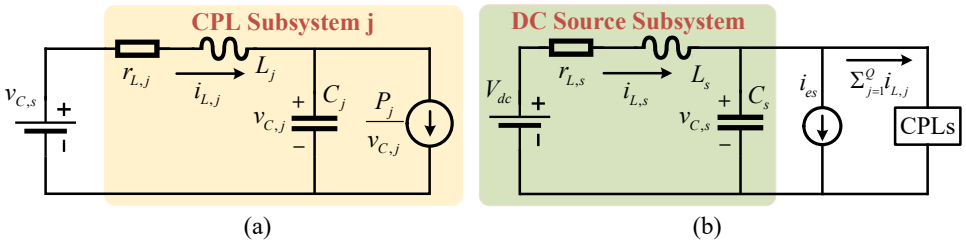

Figure 3: Simplified circuits at the CPL side (a) and the DC source side (b).

where $v_{C,j}$ and $i_{L,j}$ denote the voltage on the capacitor and the current in the inductor of the filter which is in series with the j_{th} CPL, respectively. $r_{L,j}$, L_j and C_j represent the resistance, inductance and capacitance in the filter, respectively. P_j denotes the constant load power, and the voltage-controlled current source $P_j/v_{C,j}$ refers to the CPL. $v_{C,s}$ refers to the voltage on the capacitor in the filter in the DC source subsystem, which controls the voltage of the DC bus.

Similarly, applying the Kirchhoff circuit laws to the DC source subsystem in Figure 3 (b) yields

$$\begin{cases} \dot{i}_{L,s} = \frac{1}{L_s} V_{dc} - \frac{r_s}{L_s} i_{L,s} - \frac{1}{L_s} v_{C,s} \\ \dot{v}_{C,s} = \frac{1}{C_s} i_{L,s} - \frac{1}{C_s} \Sigma_{j=1}^{Q} i_{L,j} - \frac{1}{C_s} i_{es} \end{cases} \tag{2}$$

where $v_{C,s}$ and $i_{L,s}$ represent the voltage on the capacitor and the current in the inductor in the filter in the DC source subsystem, respectively. $r_{L,s}$, C_s and L_s denote the resistance, capacitance and inductance in the filter, respectively.

Based on (1) and (2), one obtains

$$\begin{cases} \dot{x}_j(t) = \bar{A}_j x_j(t) + \bar{A}_{js} x_s(t) - d_j h_j(x_j(t)), j = 1, \ldots, Q \\ \dot{x}_s(t) = \bar{A}_s x_s(t) + \sum_{j=1}^{Q} \bar{A}_{cn} x_j(t) + b_{es} i_{es} + b_s V_{dc} \end{cases} \tag{3}$$

where $x_j(t) = col\{i_{L,j}, v_{C,j}\}$, $x_s(t) = col\{i_{L,s}, v_{C,s}\}$ and

$$\begin{cases} \bar{A}_j = \begin{bmatrix} -\frac{r_{L,j}}{L_j} & -\frac{1}{L_j} \\ \frac{1}{C_j} & 0 \end{bmatrix}, d_j = \begin{bmatrix} 0 \\ \frac{P_j}{C_j} \end{bmatrix}, \bar{A}_{js} = \begin{bmatrix} 0 & \frac{1}{L_j} \\ 0 & 0 \end{bmatrix}, h_j(x_j(t)) = \frac{1}{v_{C,j}} \\ \bar{A}_s = \begin{bmatrix} -\frac{r_s}{L_s} & -\frac{1}{L_s} \\ \frac{1}{C_s} & 0 \end{bmatrix}, b_s = \begin{bmatrix} \frac{1}{L_s} \\ 0 \end{bmatrix}, \bar{A}_{cn} = \begin{bmatrix} 0 & 0 \\ -\frac{1}{C_s} & 0 \end{bmatrix}, b_{es} = \begin{bmatrix} 0 \\ -\frac{1}{C_s} \end{bmatrix} \end{cases}$$

Remark 1. Unlike the work [20] which models the DC microgrid as a Lur'e system and uses the robust linear analysis method, the T-S fuzzy method will be introduced in the following. Due to advantages of the T-S fuzzy method in analysing nonlinear systems [21], better performance can be achieved when it handles the CPL-induced nonlinearity in DC microgrid. Besides, unlike the work [22] which focuses on the microgrid control under DoS attacks, this study will investigate the security control of the DC microgrid subject to FDI attacks, network delays and premise mismatching under the dynamic ETM scheme, which is a challenge given the complexity of the problem presented.

Using (3), the dynamic model of the DC microgrid is obtained as

$$\dot{x}(t) = \bar{A}x(t) + B_{es}i_{es}(t) - DH(x(t)) + B_sV_{dc} \tag{4}$$

where $x(t) = col\{x_1(t), x_2(t), \ldots, x_Q(t), x_s(t)\}$, $H(x(t)) = col\{h_1(x_1(t)), h_2(x_2(t)), \ldots, h_Q(x_Q(t))\}$, $B_s = col\{\underbrace{0, 0, \ldots, 0}_{Q}, b_s\}$ and

$$\bar{A} = \begin{bmatrix} \bar{A}_1 & 0 & \ldots & 0 & \bar{A}_{1s} \\ 0 & \bar{A}_2 & \ldots & 0 & \bar{A}_{2s} \\ \vdots & \vdots & \ddots & \vdots & \vdots \\ 0 & 0 & \ldots & \bar{A}_Q & \bar{A}_{Qs} \\ \bar{A}_{cn} & \bar{A}_{cn} & \ldots & \bar{A}_{cn} & \bar{A}_s \end{bmatrix}, D = \begin{bmatrix} d_1 & 0 & \ldots & 0 \\ 0 & d_2 & \ldots & 0 \\ \vdots & \vdots & \ddots & \vdots \\ 0 & 0 & \ldots & d_Q \\ 0 & 0 & \ldots & 0 \end{bmatrix}, B_{es} = \begin{bmatrix} 0 \\ 0 \\ \vdots \\ 0 \\ b_{es} \end{bmatrix}$$

To shift the equilibrium point to the origin based on a coordinate transformation, the DC microgrid model is expressed as

$$\dot{\tilde{x}}(t) = \bar{A}\tilde{x}(t) + B_{es}\tilde{i}_{es}(t) + DH(\tilde{x}(t)) \tag{5}$$

where $\tilde{x}(t) = col\{\tilde{x}_1(t), \ldots, \tilde{x}_Q(t), \tilde{x}_s(t)\} = x(t) - x_0$, $\tilde{x}_j(t) = col\{\tilde{i}_{L,j}, \tilde{v}_{C,j}\}$, $\tilde{x}_s(t) = col\{\tilde{i}_{L,s}, \tilde{v}_{C,s}\}$, $H(\tilde{x}(t)) = col\{h_1(\tilde{x}_1(t)), \ldots, h_Q(\tilde{x}_Q(t))\}$ with

$$h_j(\tilde{x}_j(t)) = \frac{\tilde{v}_{C,j}}{v_{C0,j}(\tilde{v}_{C,j} + v_{C0,j})} \tag{6}$$

where x_0 and $v_{C0,j}$ denote the equilibrium points of the DC microgrid and the voltage $v_{C,j}$, respectively.

2.2. T-S fuzzy modeling of the DC microgrid

Considering that a microgrid with several CPLs can often be transformed into a microgrid with one equivalent CPL [18], a DC microgrid with one CPL will be studied in the following. Using the sector nonlinearity approach, for the region $-\tilde{w}_{2,1} \leq \tilde{v}_{C,1} \leq \tilde{w}_{2,1}$, the nonlinear term $h_1(\tilde{x}_1(t))$ in (6) falls inside two linear sectors as follows

$$U_{min}\tilde{v}_{C,1} \leq h_1(\tilde{x}_1(t)) \leq U_{max}\tilde{v}_{C,1} \tag{7}$$

where

$$U_{min} = \frac{1}{v_{C0,1}(\tilde{w}_{2,1} + v_{C0,1})},\ U_{max} = \frac{1}{v_{C0,1}(-\tilde{w}_{2,1} + v_{C0,1})} \tag{8}$$

Based on the sector nonlinearity method, it follows from (7) that

$$\begin{cases} h_1(\tilde{x}_1(t)) = \mu_1(\tilde{x}_1(t))U_{min}\tilde{v}_{C,1} + \mu_2(\tilde{x}_1(t))U_{max}\tilde{v}_{C,1} \\ \mu_1(\tilde{x}_1(t)) + \mu_2(\tilde{x}_1(t)) = 1 \end{cases} \tag{9}$$

where membership functions $\mu_1(\tilde{x}_1(t))$ and $\mu_2(\tilde{x}_1(t))$ are derived as

$$\mu_1(\tilde{x}_1(t)) = \frac{U_{max}\tilde{v}_{C,1} - h_1(\tilde{x}_1(t))}{(U_{max} - U_{min})\tilde{v}_{C,1}},\ \mu_2(\tilde{x}_1(t)) = \frac{h_1(\tilde{x}_1(t)) - U_{min}\tilde{v}_{C,1}}{(U_{max} - U_{min})\tilde{v}_{C,1}} \tag{10}$$

Using (9), the DC microgrid system (5) can be rewritten as the T-S fuzzy model as follows

$$\dot{\tilde{x}}(t) = \sum_{i=1}^{2} \mu_i(\tilde{x}(t))\{A_i\tilde{x}(t) + B_{es}\tilde{i}_{es}\} \tag{11}$$

where

$$A_i = \begin{bmatrix} \tilde{A}_i & \bar{A}_{1s} \\ \bar{A}_{cn} & \bar{A}_s \end{bmatrix}, \tilde{A}_1 = \begin{bmatrix} -\frac{r_{L,1}}{L_1} & -\frac{1}{L_1} \\ \frac{1}{C_1} & \frac{P_1}{C_1}U_{min} \end{bmatrix}, \tilde{A}_2 = \begin{bmatrix} -\frac{r_{L,1}}{L_1} & -\frac{1}{L_1} \\ \frac{1}{C_1} & \frac{P_1}{C_1}U_{max} \end{bmatrix}$$

2.3. Dynamic event-triggered mechanism

To save communication bandwidth in the DC microgrid, a novel dynamic ETM (DETM) is proposed as

$$t_{k+1}h = t_k h + \min_{j\in\mathbb{N}}\{jh|\ jh \text{ satisfying (13) }\} \tag{12}$$

$$\begin{cases} \|\Omega^{\frac{1}{2}}(\tilde{x}(t_k h) - \tilde{x}(t_k h + jh))\|^2 > \delta(t)\|\Omega^{\frac{1}{2}}\tilde{x}(t_k h)\|^2 \\ \delta(t) = \delta_0 + \delta_d(t), \delta_d(t) = \delta_1 tanh(\varrho\|\tilde{x}(t_k h) - \tilde{x}(t_k h + jh)\|) \end{cases} \tag{13}$$

where the triggering threshold parameters $\delta_0, \delta_1 \in [0, 1)$ and $\varrho \geq 0$, positive definite matrix $\Omega > 0$, and $t_k h$ indicates the latest triggering instant.

As shown in Figure 4, at each sampling instant, the DETM determines whether or not the triggering condition in (12) is satisfied. If yes, the sampled data will be transmitted, and the sampling instant becomes the next triggering instant. Otherwise, the data will be ignored, and no new triggering instant is generated. Namely, the DETM only sends out partial data satisfying the triggering condition. Thus, the triggering instant set $\mathscr{T}_t = \{\ldots, t_k h, t_{k+1} h, \ldots\}$ is a subset of the sampling instant set $\mathscr{T}_s = \{h, 2h, \ldots\}$. Specially, if setting $\delta(t) = 0$, the triggering condition is satisfied at each sampling instant, and thus the DETM becomes the time-triggered mechanism (TTM) (i.e., periodic sampling mode).

Remark 2. For an ETC system, it is essential to ensure a positive minimum inter-event time (MIET). Otherwise, the Zeno behavior will occur, i.e., an infinite number of events will be generated in finite time [23], which makes the ETC system ineffective or even useless in practice. Unlike the continuous-time ETMs [14, 15, 16] which require extensive computation to guarantee a positive MIET, the MIET of the proposed discrete-time ETM (12) is not less than the sampling period, which excludes Zeno behavior naturally.

Remark 3. Unlike the static ETM (SETM) which uses a fixed threshold parameter [17, 24], the proposed DETM (12) uses a dynamic threshold term $\delta_d(t)$, which changes adaptively with the state error norm. During the transient response, the large state error results in a large $\delta(t)$, which helps the DETM save more communication resources than the SETM. Besides, the SETM can be seen as a special case of the DETM with $\delta_d(t) = 0$.

2.4. Closed-loop system modeling

Considering the network induced delays, the updating instants of the current injection controller can be expressed as $\{\ldots, t_k + \tau_k, t_{k+1} + \tau_{k+1}, \ldots\}$, where the delay τ_k satisfies $\tau_k \in [\tau_m, \tau_M]$.

Divide the updating intervals of the controller as (as shown in Figure 4)

$$[t_k h + \tau_k, t_{k+1} h + \tau_{k+1}) = \bigcup_{\ell_k=0}^{\epsilon_k} \phi_{\ell_k}^{t_k} \tag{14}$$

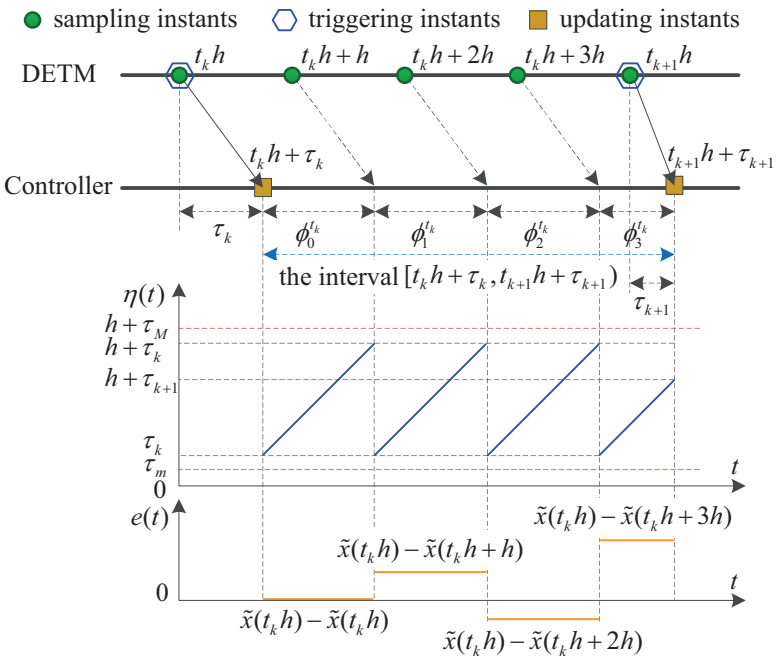

Figure 4: Division of the updating intervals of the controller.

where $\epsilon_k = t_{k+1} - t_k - 1$, $\bar{\phi}_{\ell_k}^{t_k} = t_k h + \ell_k h + \tau_k$ and

$$\phi_{\ell_k}^{t_k} = \begin{cases} [\bar{\phi}_{\ell_k}^{t_k}, \bar{\phi}_{\ell_k}^{t_k} + h), \ \ell_k = 0, 1, \ldots, \epsilon_k - 1 \\ [\bar{\phi}_{\ell_k}^{t_k}, t_{k+1} h + \tau_{k+1}), \ \ell_k = \epsilon_k \end{cases} \tag{15}$$

Define the state error function $e(t)$ and the artificial delay function $\eta(t)$ as (as shown in Figure 4)

$$\eta(t) = t - (t_k h + \ell_k h), \ e(t) = \tilde{x}(t_k h) - \tilde{x}(t_k h + \ell_k h), \ t \in \phi_{\ell_k}^{t_k} \tag{16}$$

where $e(t)$ is a piecewise-constant function, and $\eta(t)$ satisfies $\eta(t) \in [\tau_k, max\{h + \tau_k, h + \tau_{k+1}\}) \subseteq [\tau_m, h + \tau_M)$ and $\dot{\eta}(t) = 1(t \in \phi_{\ell_k}^{t_k} \backslash (t_k h + \tau_k + \ell_k h))$.

Using $e(t)$ and $\eta(t)$ in (16), the controller input (i.e., transmitted data of the DETM) can be described as

$$\bar{x}(t) = \tilde{x}(t_k h) = e(t) + \tilde{x}(t - \eta(t)), \ t \in \phi_{\ell_k}^{t_k} \tag{17}$$

Considering effects of the DETM, the controller can not share the same premise variables as the fuzzy model of the microgrid, so the event-triggered

fuzzy injection current controller is designed as

$$\tilde{i}_{es} = \sum_{j=1}^{2} \bar{\mu}_j(\bar{x}(t)) K_j \bar{x}(t),\ t \in \phi_{\ell_k}^{t_k} \tag{18}$$

where

$$\begin{cases} \bar{\mu}_1(\bar{x}(t)) = \frac{U_{max}\bar{v}_{C,1} - h_1(\bar{x}(t))}{(U_{max} - U_{min})\bar{v}_{C,1}}, \bar{\mu}_2(\bar{x}(t)) = 1 - \bar{\mu}_1(\bar{x}(t)) \\ h_1(\bar{x}(t)) = \frac{\bar{v}_{C,1}}{v_{C0,1}(\bar{v}_{C,1} + v_{C0,1})},\ \ \bar{v}_{C,1} = \tilde{v}_{C,1}(t_k h) \end{cases}$$

Remark 4. As shown in Figure 2, due to the DETM and communication network, the injection current controller (18) can not share the same premise with the microgrid. Thus, the premise mismatching issue is considered in this paper when designing the controller (18), which is more comprehensive and practical than the methods presented in [18, 19] which assume the perfect premise matching. To deal with the premise mismatching issue, the slack matrices $\Psi^i (i = 1, 2)$ will be introduced in Theorem 1, which helps to establish the relationship between the premises $\bar{\mu}_j (j = 1, 2)$ and μ_j.

Further, considering effects of the random FDI attacks, based on the controller (18), the event-triggered fuzzy security injection current (ETFSIC) controller can be expressed as

$$\tilde{i}_{es} = \sum_{j=1}^{2} \bar{\mu}_j(\bar{x}(t)) K_j \bar{x}(t) + \alpha(t)\mathscr{F}(t),\ t \in \phi_{\ell_k}^{t_k} \tag{19}$$

where $\mathscr{F}(t) = f(\bar{x}(t))$ is the FDI attack function, and the Bernoulli distribution $\alpha(t) \in \{0, 1\}$ has an expectation $\mathbb{E}\{\alpha(t)\} = \bar{\alpha}$. If the attack is active (i.e., $\alpha(t) = 1$), the control signal will be tampered, whereas the control signal will not be affected if the attack is sleeping (i.e., $\alpha(t) = 0$).

To reduce the chance of being detected by surveillance and security systems, adversaries often limit the attack energy as [25]

$$\mathscr{F}^T(t)\mathscr{F}(t) \leq \bar{x}^T(t) G^T G \bar{x}(t) \tag{20}$$

where G is the upper bound of the nonlinearity.

Using the DC microgrid model (11) and the current injection fuzzy controller (19), the closed-loop fuzzy system model is achieved as

$$\begin{aligned}\dot{\tilde{x}}(t) = & \sum_{i=1}^{2}\sum_{j=1}^{2}\mu_i\bar{\mu}_j[A_i\tilde{x}(t) + B_{es}K_j(\tilde{x}(t-\eta(t)) + e(t)) \\ & + B_{es}\bar{\alpha}\mathscr{F}(t) + B_{es}(\alpha(t)-\bar{\alpha})\mathscr{F}(t)]\end{aligned} \tag{21}$$

where $\mu_i = \mu_i(\tilde{x}(t))$ and $\bar{\mu}_j = \bar{\mu}_j(\bar{x}(t))$ are defined to ensure a compact format.

Remark 5. Unlike the works [18, 19] which assume perfect premise matching, the system model (21) is more generic, which makes it possible to comprehensively study the effects of the FDI attacks, the dynamic ETM, network delays, premise mismatching and CPL-induced nonlinear issue all in one unified framework. Besides, unlike the active damping method which only guarantees small signal stability, the T-S fuzzy system model (21) can be used for the following large signal stability analysis.

3. Stability analysis of the DC microgrid

Definition 1. [26] For the solution of the system (21) with the initial condition $\mathscr{C}$, if there exist $a_1 > 0$ and $a_2 \in [0, 1)$ satisfying

$$\mathbb{E}\{\|\tilde{x}(t)\|^2\} \leq a_1\|\mathscr{C}\|^2 a_2^t,\ t \geq 0 \tag{22}$$

then, the system is said to be mean-square exponentially stable.

For simplification, define

$$\begin{cases} e_i = [\ \overbrace{0\ \ldots\ 0}^{i-1}\ I\ \overbrace{0\ \ldots\ 0}^{6-i}\ ]\ (i = 1, \ldots, 6) \\ \xi(t) = col\{\tilde{x}(t), \tilde{x}(t-\eta_1), \tilde{x}(t-\eta(t)), \tilde{x}(t-\eta_2), e(t), \mathscr{F}(t)\} \end{cases} \tag{23}$$

Theorem 1. For given sampling period h, delay bounds $0 \leq \tau_m \leq \tau_M$, attack expectation $\bar{\alpha} \in [0, 1]$ and attack-related matrix G, threshold parameters $(\delta_0, \delta_1 \in [0, 1))$ of the DETM, decay rate $\sigma > 0$, and scalars $\rho_j \in (0, 1)(j = 1, 2)$ satisfying $\bar{\mu}_j \geq \rho_j\mu_j$, if there exist matrices $P > 0, S >$

$0, Q > 0, R_1 > 0, R_2 > 0, \Omega > 0$, symmetric matrices $\Psi^i (i = 1, 2)$ and matrix U satisfying

$$\begin{bmatrix} R_2 & * \\ U & R_2 \end{bmatrix} > 0 \tag{24}$$

$$\Upsilon^{ij} - \Psi^i < 0,\ 1 \le i, j \le 2 \tag{25}$$

$$\rho_i(\Upsilon^{ii} - \Psi^i) + \Psi^i < 0,\ i = 1, 2 \tag{26}$$

$$\rho_j(\Upsilon^{ij} - \Psi^i) + \rho_i(\Upsilon^{ji} - \Psi^j) + \Psi^i + \Psi^j < 0,\ 1 \le i < j \le 2 \tag{27}$$

where

$$\Upsilon^{ij} = \begin{bmatrix} \Upsilon_{11}^{ij} & * & * & * \\ \Upsilon_{21}^{ij} & \Upsilon_{22} & * & * \\ \Upsilon_{31} & 0 & \Upsilon_{33} & * \\ \Upsilon_{41} & 0 & 0 & \Upsilon_{44} \end{bmatrix},$$

$\Upsilon_{11}^{ij} = \Xi^{ij} - \Lambda_1^{ijT}(\eta_1^2 R_1 + \eta_{21}^2 R_2)\Lambda_1^{ij} - \tilde{\alpha}^2 \Lambda_2^T(\eta_1^2 R_1 + \eta_{21}^2 R_2)\Lambda_2 - e_5^T \Omega e_5 - \bar{\alpha} e_6^T e_6$,
$\Upsilon_{21}^{ij} = \begin{bmatrix} \eta_1 \Lambda_1^{ij} \\ \eta_{21}\Lambda_1^{ij} \end{bmatrix}$, $\Upsilon_{31} = \tilde{\alpha} \begin{bmatrix} \eta_1 \Lambda_2 \\ \eta_{21}\Lambda_2 \end{bmatrix}$, $\Upsilon_{41} = \begin{bmatrix} \delta^{0.5}(e_3 + e_5) \\ G(e_3 + e_5) \end{bmatrix}$,
$\Upsilon_{22} = \Upsilon_{33} = \begin{bmatrix} -R_1^{-1} & * \\ 0 & -R_2^{-1} \end{bmatrix}$, $\Upsilon_{44} = \begin{bmatrix} -\Omega^{-1} & * \\ 0 & -\bar{\alpha}^{-1} \end{bmatrix}$,
$\Lambda_1^{ij} = A_i e_1 + B_{es} K_j (e_3 + e_5) + \bar{\alpha} B_{es} e_6, \Lambda_2 = B_{es} e_6$,
$\Xi^{ij} = \sigma e_1^T P e_1 + He\{e_1^T P \Lambda_1^{ij}\} + e_1^T S e_1 - e^{-\sigma\eta_1} e_2^T S e_2 + e^{-\sigma\eta_1} e_2^T Q e_2 - e^{-\sigma\eta_2} e_4^T Q e_4 + \Lambda_1^{ijT}(\eta_1^2 R_1 + \eta_{21}^2 R_2)\Lambda_1^{ij} + \tilde{\alpha}^2 \Lambda_2^T(\eta_1^2 R_1 + \eta_{21}^2 R_2)\Lambda_2 - e^{-\sigma\eta_1}(e_1 - e_2)^T R_1 (e_1 - e_2) - e^{-\sigma\eta_2}(e_2 - e_3)^T R_2 (e_2 - e_3) - e^{-\sigma\eta_2}(e_3 - e_4)^T R_2 (e_3 - e_4) - e^{-\sigma\eta_2} He\{(e_3 - e_4)^T U (e_2 - e_3)\}$, $\tilde{\alpha} = (\bar{\alpha}(1 - \bar{\alpha}))^{0.5}$,
then, the DC microgrid system (21) under the FDI attacks, the DETM, network delays and imperfect premise matching is mean-square exponentially stable.

Proof. Construct a Lyapunov-Krasovskii functional (LKF) as

$$\begin{aligned} V(t) =& \tilde{x}^T(t) P \tilde{x}(t) + \eta_1 \int_{-\eta_1}^{0} \int_{t+s}^{t} e^{\sigma(\theta - t)} \dot{\tilde{x}}^T(\theta) R_1 \dot{\tilde{x}}(\theta) d\theta ds \\ &+ \int_{t-\eta_2}^{t-\eta_1} e^{\sigma(\theta - t)} \tilde{x}^T(\theta) Q \tilde{x}(\theta) d\theta + \int_{t-\eta_1}^{t} e^{\sigma(\theta - t)} \tilde{x}^T(\theta) S \tilde{x}(\theta) d\theta \\ &+ \eta_{21} \int_{-\eta_2}^{-\eta_1} \int_{t+s}^{t} e^{\sigma(\theta - t)} \dot{\tilde{x}}^T(\theta) R_2 \dot{\tilde{x}}(\theta) d\theta ds \end{aligned} \tag{28}$$

where positive definite matrices $P > 0, S > 0, Q > 0, R_1 > 0$ and $R_2 > 0$, scalars $\eta_1 = \tau_m, \eta_2 = h + \tau_M$, and $\eta_{21} = \eta_2 - \eta_1$.

Taking the time derivative of $V(t)$ yields

$$\begin{aligned}\dot{V}(t) \leq & -\sigma V(t) - e^{-\sigma\eta_1}\tilde{x}^T(t-\eta_1)S\tilde{x}(t-\eta_1) + \tilde{x}^T(t)S\tilde{x}(t) \\ & + He\{\tilde{x}^T(t)P\dot{\tilde{x}}(t)\} + \sigma\tilde{x}^T(t)P\tilde{x}(t) \\ & - e^{-\sigma\eta_2}\tilde{x}^T(t-\eta_2)Q\tilde{x}(t-\eta_2) + e^{-\sigma\eta_1}\tilde{x}^T(t-\eta_1)Q\tilde{x}(t-\eta_1) \\ & + \zeta_1(t) + \zeta_2(t) + \dot{\tilde{x}}^T(t)(\eta_1^2 R_1 + \eta_{21}^2 R_2)\dot{\tilde{x}}(t)\end{aligned} \tag{29}$$

where

$$\begin{cases}\zeta_1(t) = -\eta_1 e^{-\sigma\eta_1}\int_{t-\eta_1}^{t}\dot{\tilde{x}}^T(s)R_1\dot{\tilde{x}}(s)ds \\ \zeta_2(t) = -\eta_{21}e^{-\sigma\eta_2}\int_{t-\eta_2}^{t-\eta_1}\dot{\tilde{x}}^T(s)R_2\dot{\tilde{x}}(s)ds\end{cases} \tag{30}$$

Using Jensen inequality to $\zeta_1(t)$ and $\zeta_2(t)$, and then using reciprocally convex method [27] together with (24) to $\zeta_2(t)$, we have

$$\begin{cases}\zeta_1(t) \leq -e^{-\sigma\eta_1}(\tilde{x}(t) - \tilde{x}(t-\eta_1))^T R_1(\tilde{x}(t) - \tilde{x}(t-\eta_1)) \\ \zeta_2(t) = -\eta_{21}e^{-\sigma\eta_2}\left[\int_{t-\eta(t)}^{t-\eta_1}\mathscr{R}(s)ds + \int_{t-\eta_2}^{t-\eta(t)}\mathscr{R}(s)ds\right] \\ \qquad \leq -e^{-\sigma\eta_2}(\varphi_1^T R_2\varphi_1 - \varphi_2^T R_2\varphi_2 - He\{\varphi_2^T U\varphi_1\})\end{cases} \tag{31}$$

where $\varphi_1 = [\tilde{x}(t-\eta_1) - \tilde{x}(t-\eta(t))]$, $\varphi_2 = [\tilde{x}(t-\eta(t)) - \tilde{x}(t-\eta_2)]$ and $\mathscr{R}(\theta) = \dot{\tilde{x}}^T(\theta)R_2\dot{\tilde{x}}(\theta)$.

Substituting (31) into (29), and computing the mathematical expectation, we have

$$\mathbb{E}\{\dot{V}(t)\} \leq -\sigma\mathbb{E}\{V(t)\} + \sum_{i=1}^{2}\sum_{j=1}^{2}\mu_i\bar{\mu}_j\xi^T(t)\Xi^{ij}\xi(t) \tag{32}$$

Using (32), the following equivalent inequality holds

$$\begin{aligned}\mathbb{E}\{\dot{V}(t)\} \leq & -\sigma\mathbb{E}\{V(t)\} + \sum_{i=1}^{2}\sum_{j=1}^{2}\mu_i\bar{\mu}_j\left[\xi^T(t)\Xi^{ij}\xi(t) + e^T(t)\Omega e(t)\right. \\ & \left. + \bar{\alpha}\mathscr{F}^T(t)\mathscr{F}(t) - e^T(t)\Omega e(t) - \bar{\alpha}\mathscr{F}^T(t)\mathscr{F}(t)\right]\end{aligned} \tag{33}$$

Using the triggering condition (13) of the DETM and the attack related

condition (20), it follows from (33) that

$$\begin{aligned}
&\mathbb{E}\{\dot{V}(t)\} + \sigma\mathbb{E}\{V(t)\} \\
&\leq \sum_{i=1}^{2}\sum_{j=1}^{2} \mu_i\bar{\mu}_j \left[\xi^T(t)\Xi^{ij}\xi(t) - \bar{\alpha}\mathscr{F}^T(t)\mathscr{F}(t) - e^T(t)\Omega e(t)\right. \\
&\quad \left. + (\tilde{x}(t-\eta(t)) + e(t))^T(\delta\Omega + \bar{\alpha}G^TG)(\tilde{x}(t-\eta(t)) + e(t))\right. \\
&\leq \sum_{i=1}^{2}\sum_{j=1}^{2} \mu_i\bar{\mu}_j\xi^T(t)\Upsilon^{ij}\xi(t)
\end{aligned} \tag{34}$$

where $\Upsilon^{ij} = \Xi^{ij} - e_5^T\Omega e_5 - \bar{\alpha}e_6^Te_6 + (e_3+e_5)^T(\delta\Omega + \bar{\alpha}G^TG)(e_3+e_5)$.

To handle the imperfect premise matching issue [28], using $\sum_{j=1}^{2}\mu_j = \sum_{j=1}^{2}\bar{\mu}_j = 1$, the following equation holds

$$\sum_{i=1}^{2}\mu_i\left(\sum_{j=1}^{2}\mu_j - \sum_{j=1}^{2}\bar{\mu}_j\right)\xi^T(t)\Psi^i\xi(t) = 0 \tag{35}$$

Using (35), it follows from (34) that

$$\begin{aligned}
&\sum_{i=1}^{2}\sum_{j=1}^{2}\mu_i\bar{\mu}_j\xi^T(t)\Upsilon^{ij}\xi(t) \\
&= \sum_{i=1}^{2}\sum_{j=1}^{2}\mu_i\bar{\mu}_j\xi^T(t)\Upsilon^{ij}\xi(t) + \sum_{i=1}^{2}\sum_{j=1}^{2}\mu_i(\mu_j - \bar{\mu}_j)\xi^T(t)\Psi^i\xi(t) \\
&= \sum_{i=1}^{2}\sum_{j=1}^{2}\mu_i\bar{\mu}_j\xi^T(t)(\Upsilon^{ij} - \Psi^i)\xi(t) + \sum_{i=1}^{2}\sum_{j=1}^{2}\mu_i\mu_j\xi^T(t)\Psi^i\xi(t)
\end{aligned} \tag{36}$$

Using (25) and $\bar{\mu}_j \geq \rho_j\mu_j$, if follows from (36) that

$$\begin{aligned}
&\sum_{i=1}^{2}\sum_{j=1}^{2}\mu_i\bar{\mu}_j\xi^T(t)\Upsilon^{ij}\xi(t) \\
&\leq \sum_{i=1}^{2}\sum_{j=1}^{2}\mu_i\mu_j\xi^T(t)\rho_j(\Upsilon^{ij} - \Psi^i)\xi(t) + \sum_{i=1}^{2}\sum_{j=1}^{2}\mu_i\mu_j\xi^T(t)\Psi^i\xi(t) \\
&\leq \sum_{i=1}^{2}\mu_i\mu_i\xi^T(t)\left[\rho_i(\Upsilon^{ii} - \Psi^i) + \Psi^i\right]\xi(t) + \sum_{i=1}^{2}\sum_{j>i}^{2}\mu_i\mu_j\xi^T(t) \\
&\quad \left[\rho_j(\Upsilon^{ij} - \Psi^i) + \rho_i(\Upsilon^{ji} - \Psi^j) + \Psi^i + \Psi^j\right]\xi(t)
\end{aligned} \tag{37}$$

Substituting (26) and (27) into (37) yields $\sum_{i=1}^{2}\sum_{j=1}^{2}\mu_i\bar{\mu}_j\xi^T(t)\Upsilon^{ij}\xi(t) \leq 0$, and thus it follows from (34) that

$$\begin{cases}\mathbb{E}\{\dot{V}(t)\}+\sigma\mathbb{E}\{V(t)\}\leq 0\\ \Rightarrow\ \mathbb{E}\{\|\tilde{x}(t)\|^2\}\leq\lambda_{\min}^{-1}(P)\mathbb{E}\{V(0)\}e^{-\sigma t},\ \forall t\geq 0\end{cases} \tag{38}$$

Using Definition 1, one derives from (38) that the DC microgrid system (21) under the FDI attacks, the DETM, network delays and imperfect premise matching is mean-square exponentially stable. The proof is thus completed.

Specially, without considering the deception attacks, the DC microgrid system (21) changes into

$$\dot{\tilde{x}}(t)=\sum_{i=1}^{2}\sum_{j=1}^{2}\mu_i\bar{\mu}_j[A_i\tilde{x}(t)+B_{es}K_j(\tilde{x}(t-\eta(t))+e(t))] \tag{39}$$

Corollary 1. For the given sampling period h, delay bounds $0\leq\tau_m\leq\tau_M$, threshold parameters $(\delta_0,\delta_1\in[0,1))$ of the DETM, decay rate $\sigma>0$, and scalars $\rho_j\in(0,1)(j=1,2)$ satisfying $\bar{\mu}_j\geq\rho_j\mu_j$, if there exist positive definite matrices $P>0,S>0,Q>0,R_1>0,R_2>0,\Omega>0$, symmetric matrices $\tilde{\Psi}^i(i=1,2)$ and matrix U satisfying (24) and

$$\tilde{\Upsilon}^{ij}-\tilde{\Psi}^i<0,\ 1\leq i,j\leq 2 \tag{40}$$

$$\rho_i(\tilde{\Upsilon}^{ii}-\tilde{\Psi}^i)+\tilde{\Psi}^i<0,\ i=1,2 \tag{41}$$

$$\rho_j(\tilde{\Upsilon}^{ij}-\tilde{\Psi}^i)+\rho_i(\tilde{\Upsilon}^{ji}-\tilde{\Psi}^j)+\tilde{\Psi}^i+\tilde{\Psi}^j<0,\ 1\leq i<j\leq 2 \tag{42}$$

where

$$\tilde{\Upsilon}^{ij}=\begin{bmatrix}\tilde{\Upsilon}_{11}^{ij} & * & * & *\\ \eta_1\tilde{\Lambda}_1^{ij} & -R_1^{-1} & * & *\\ \eta_{21}\tilde{\Lambda}_1^{ij} & 0 & -R_2^{-1} & *\\ \sqrt{\delta}(\tilde{e}_3+\tilde{e}_5) & 0 & 0 & -\Omega^{-1}\end{bmatrix},$$

$\tilde{\Upsilon}_{11}^{ij}=\sigma\tilde{e}_1^TP\tilde{e}_1+He\{\tilde{e}_1^TP\tilde{\Lambda}_1^{ij}\}+\tilde{e}_1^TS\tilde{e}_1-e^{-\sigma\eta_1}\tilde{e}_2^TS\tilde{e}_2+e^{-\sigma\eta_1}\tilde{e}_2^TQ\tilde{e}_2-e^{-\sigma\eta_2}\tilde{e}_4^TQ\tilde{e}_4-e^{-\sigma\eta_1}(\tilde{e}_1-\tilde{e}_2)^TR_1(\tilde{e}_1-\tilde{e}_2)-e^{-\sigma\eta_2}(\tilde{e}_2-\tilde{e}_3)^TR_2(\tilde{e}_2-\tilde{e}_3)-e^{-\sigma\eta_2}(\tilde{e}_3-\tilde{e}_4)^TR_2(\tilde{e}_3-\tilde{e}_4)-e^{-\sigma\eta_2}He\{(\tilde{e}_3-\tilde{e}_4)^TU(\tilde{e}_2-\tilde{e}_3)\}-\tilde{e}_5^T\Omega\tilde{e}_5,$

$\tilde{\Lambda}_1^{ij}=A_i\tilde{e}_1+B_{es}K_j(\tilde{e}_3+\tilde{e}_5),$

then, the DC microgrid system (39) under the DETM, network delays and imperfect premise matching is exponentially stable.

PROOF. Use the LKF (28) and define

$$\begin{cases} \tilde{e}_i = [\ \overbrace{0\ \ldots\ 0}^{i-1}\ I\ \overbrace{0\ \ldots\ 0}^{5-i}\ ]\ (i = 1, \ldots, 5) \\ \tilde{\xi}(t) = col\{\tilde{x}(t), \tilde{x}(t-\eta_1), \tilde{x}(t-\eta(t)), \tilde{x}(t-\eta_2), e(t)\} \end{cases}$$

The proof is similar to that of Theorem 1, which is omitted here.

Specially, if setting $\delta(t) = 0$, the DETM becomes the TTM. When using a small sampling period, a parallel distributed compensation (PDC) technology is often adopted in T-S fuzzy control. Using the TTM and PDC technology, the DC microgrid system (39) changes into

$$\dot{\tilde{x}}(t) = \sum_{i=1}^{2} \mu_i [A_i \tilde{x}(t) + B_{es} K_i \tilde{x}(t - \eta(t))] \tag{43}$$

PROOF. Considering that the TTM results in $e(t) = 0$, and using the PDC technology with the common B_{es}, the DC microgrid system (39) can be rewritten as

$$\begin{aligned} \dot{\tilde{x}}(t) &= \sum_{i=1}^{2} \sum_{j=1}^{2} \mu_i \mu_j [A_i \tilde{x}(t) + B_{es} K_j \tilde{x}(t - \eta(t))] \\ &= \sum_{i=1}^{2} \mu_i [A_i \tilde{x}(t) + B_{es} K_i \tilde{x}(t - \eta(t))] \end{aligned} \tag{44}$$

The proof is thus completed.

Corollary 2. For given sampling period h, delay bounds $0 \leq \tau_m \leq \tau_M$, decay rate $\sigma > 0$, if there exist matrices $P > 0, S > 0, Q > 0, R_1 > 0, R_2 > 0$, and matrix U satisfying (24) and

$$\begin{bmatrix} \hat{\Upsilon}_{11}^{ii} & * & * \\ \eta_1 \hat{\Lambda}_1^{ii} & -R_1^{-1} & * \\ \eta_{21} \hat{\Lambda}_1^{ii} & 0 & -R_2^{-1} \end{bmatrix} < 0,\ i = 1, 2 \tag{45}$$

where
$\hat{\Upsilon}_{11}^{ii} = \sigma \hat{e}_1^T P \hat{e}_1 + He\{\hat{e}_1^T P \hat{\Lambda}_1^{ii}\} + \hat{e}_1^T S \hat{e}_1 - e^{-\sigma\eta_1} \hat{e}_2^T S \hat{e}_2 + e^{-\sigma\eta_1} \hat{e}_2^T Q \hat{e}_2 - e^{-\sigma\eta_2} \hat{e}_4^T Q \hat{e}_4 - e^{-\sigma\eta_1} (\hat{e}_1 - \hat{e}_2)^T R_1 (\hat{e}_1 - \hat{e}_2) - e^{-\sigma\eta_2} (\hat{e}_2 - \hat{e}_3)^T R_2 (\hat{e}_2 - \hat{e}_3) - e^{-\sigma\eta_2} (\hat{e}_3 - \hat{e}_4)^T R_2 (\hat{e}_3 -$

$\hat{e}_4) - e^{-\sigma\eta_2} He\{(\hat{e}_3 - \hat{e}_4)^T U(\hat{e}_2 - \hat{e}_3)\}$,
$\hat{\Lambda}_1^{ii} = A_i\hat{e}_1 + B_{es}K_i\hat{e}_3,\ \ \hat{e}_i = [\ \overbrace{0\ \ldots\ 0}^{i-1}\ I\ \overbrace{0\ \ldots\ 0}^{4-i}\ ]\ (i = 1, \ldots, 4)$,
then, the DC microgrid system (43) under the TTM and network delays is exponentially stable.

PROOF. Using the LKF (28), similar to (34), one obtains the following inequality

$$\mathbb{E}\{\dot{V}(t)\} + \sigma\mathbb{E}\{V(t)\} \leq \sum_{i=1}^{2} \mu_i \hat{\xi}^T(t)\hat{\Upsilon}^{ii}\hat{\xi}(t) \tag{46}$$

where $\hat{\xi}(t) = col\{\tilde{x}(t), \tilde{x}(t-\eta_1), \tilde{x}(t-\eta(t)), \tilde{x}(t-\eta_2)\}$.

Using Schur complement to (45) yields

$$\hat{\Upsilon}^{ii} = \hat{\Upsilon}_{11}^{ii} + \hat{\Lambda}_1^{ii^T}(\eta_1^2 R_1 + \eta_{21}^2 R_2)\hat{\Lambda}_1^{ii} < 0,\ i = 1, 2 \tag{47}$$

Substituting (47) into (46) yields $\mathbb{E}\{\dot{V}(t)\} + \sigma\mathbb{E}\{V(t)\} \leq 0$. Thus, the DC microgrid system (43) under the TTM and network delays is exponentially stable. This completes the proof.

In Theorem 1 and Corollaries, gain matrices (K_1, K_2) of the current injection fuzzy controller (18) and the matrix P are coupled, which makes it necessary to provide the controller design method in the following.

4. Co-design of the ETFSIC controller and DETM

Lemma 1. For a constant $\varepsilon > 0$ and matrices $Q > 0$ and X, the following inequality holds

$$-XQ^{-1}X \leq \varepsilon^2 Q - 2\varepsilon X \tag{48}$$

PROOF. For a given $Q > 0$, we have $(X - \varepsilon Q)Q^{-1}(X - \varepsilon Q) \geq 0$, which implies $-XQ^{-1}X \leq \varepsilon^2 Q - 2\varepsilon X$.

Theorem 2. For given sampling period h, delay bounds $0 \leq \tau_m \leq \tau_M$, attack expectation $\bar{\alpha} \in [0, 1]$ and attack-related matrix G, threshold parameters $(\delta_0, \delta_1 \in [0, 1))$ of the DETM, decay rate $\sigma > 0$, scalars $\varepsilon_i > 0 (i = 1, \ldots, 5)$,

and $\rho_j \in (0,1)(j=1,2)$ satisfying $\bar{\mu}_j \geq \rho_j \mu_j$, if there exist positive definite matrices $X>0, \bar{S}>0, \bar{Q}>0, \bar{R}_1>0, \bar{R}_2>0, \bar{\Omega}>0$, symmetric matrices $\bar{\Psi}^i(i=1,2)$, and matrices U and $Y_j(j=1,2)$ satisfying

$$\begin{bmatrix} \bar{R}_2 & * \\ \bar{U} & \bar{R}_2 \end{bmatrix} > 0 \tag{49}$$

$$\bar{\Upsilon}^{ij} - \bar{\Psi}^i < 0,\ 1 \leq i,j \leq 2 \tag{50}$$

$$\rho_i(\bar{\Upsilon}^{ii} - \bar{\Psi}^i) + \bar{\Psi}^i < 0,\ i=1,2 \tag{51}$$

$$\rho_j(\bar{\Upsilon}^{ij} - \bar{\Psi}^i) + \rho_i(\bar{\Upsilon}^{ji} - \bar{\Psi}^j) + \bar{\Psi}^i + \bar{\Psi}^j < 0,\ 1 \leq i < j \leq 2 \tag{52}$$

where

$$\bar{\Upsilon}^{ij} = \begin{bmatrix} \bar{\Upsilon}_{11}^{ij} & * & * & * \\ \bar{\Upsilon}_{21}^{ij} & \bar{\Upsilon}_{22} & * & * \\ \bar{\Upsilon}_{31} & 0 & \bar{\Upsilon}_{33} & * \\ \bar{\Upsilon}_{41} & 0 & 0 & \bar{\Upsilon}_{44} \end{bmatrix} \tag{53}$$

$\bar{\Upsilon}_{11}^i = \sigma e_1^T X e_1 + He\{e_1^T \bar{\Lambda}_1^{ij}\} + e_1^T \bar{S} e_1 - e^{-\sigma\eta_1} e_2^T \bar{S} e_2 + e^{-\sigma\eta_1} e_2^T \bar{Q} e_2 - e^{-\sigma\eta_2} e_4^T \bar{Q} e_4 - e^{-\sigma\eta_1}(e_1-e_2)^T \bar{R}_1 (e_1-e_2) - e^{-\sigma\eta_2}(e_2-e_3)^T \bar{R}_2 (e_2-e_3) - e^{-\sigma\eta_2}(e_3-e_4)^T \bar{R}_2 (e_3-e_4) - e^{-\sigma\eta_2} He\{(e_3-e_4)^T \bar{U}(e_2-e_3)\} - e_5^T \bar{\Omega} e_5 - \bar{\alpha} e_6^T e_6$,
$\bar{\Upsilon}_{21}^{ij} = \begin{bmatrix} \eta_1 \bar{\Lambda}_1^{ij} \\ \eta_{21} \bar{\Lambda}_1^{ij} \end{bmatrix}$, $\bar{\Upsilon}_{22} = \begin{bmatrix} \varepsilon_1^2 R_1 - 2\varepsilon_1 X & * \\ 0 & \varepsilon_2^2 R_2 - 2\varepsilon_2 X \end{bmatrix}$,
$\bar{\Upsilon}_{31} = \tilde{\alpha} \begin{bmatrix} \eta_1 \bar{\Lambda}_2 \\ \eta_{21} \bar{\Lambda}_2 \end{bmatrix}$, $\bar{\Upsilon}_{33} = \begin{bmatrix} \varepsilon_3^2 R_1 - 2\varepsilon_3 X & * \\ 0 & \varepsilon_4^2 R_2 - 2\varepsilon_4 X \end{bmatrix}$,
$\bar{\Upsilon}_{41} = \begin{bmatrix} \delta^{0.5} X(e_3+e_5) \\ GX(e_3+e_5) \end{bmatrix}$, $\bar{\Upsilon}_{44} = \begin{bmatrix} \varepsilon_5^2 \bar{\Omega} - 2\varepsilon_5 X & * \\ 0 & -\bar{\alpha}^{-1} \end{bmatrix}$,
$\bar{\Lambda}_1^{ij} = A_i X e_1 + B_{es} Y_j (e_3+e_5) + \bar{\alpha} B_{es} e_6$, $\bar{\Lambda}_2 = B_{es} e_6$,
$\bar{\Psi}^i = \Phi_2^T \Psi^i \Phi_2 (i=1,2)$, $\bar{S} = XSX, \bar{Q} = XQX, \bar{R}_1 = XR_1X, \bar{R}_2 = XR_2X, \bar{U} = XUX, \bar{\Omega} = X\Omega X, Y_j = K_j X (j=1,2)$,
then, the DC microgrid system (21) under the FDI attacks, the DETM, network delays and imperfect premise matching is mean-square exponentially stable, and the gain matrices of the current injection fuzzy controller (18) are obtained as $K_j = Y_j X^{-1} (j=1,2)$.

Proof. Define the matrices as follows

$$X = P^{-1},\ \Phi_1 = diag\{X, X\},\ \Phi_2 = diag\{\underbrace{X, \ldots, X}_{5}, \underbrace{I, \ldots, I}_{7}\} \tag{54}$$

Applying the following transform to the conditions in the Theorem 1 yields

$$\begin{bmatrix} \bar{R}_2 & * \\ \bar{U} & \bar{R}_2 \end{bmatrix} = \Phi_1 \begin{bmatrix} R_2 & * \\ U & R_2 \end{bmatrix} \Phi_1 > 0 \tag{55}$$

$$\check{\Upsilon}^{ij} - \bar{\Psi}^i = \Phi_2^T(\Upsilon^{ij} - \Psi^i)\Phi_2 < 0,\ 1 \le i, j \le 2 \tag{56}$$

$$\rho_i(\check{\Upsilon}^{ii} - \bar{\Psi}^i) + \bar{\Psi}^i = \Phi_2^T(\rho_i(\Upsilon^{ii} - \Psi^i) + \Psi^i)\Phi_2 < 0,\ i = 1, 2 \tag{57}$$

$$\begin{aligned} &\rho_j(\check{\Upsilon}^{ij} - \bar{\Psi}^i) + \rho_i(\check{\Upsilon}^{ji} - \bar{\Psi}^j) + \bar{\Psi}^i + \bar{\Psi}^j = \Phi_2^T(\rho_j(\Upsilon^{ij} - \Psi^i) \\ &+ \rho_i(\Upsilon^{ji} - \Psi^j) + \Psi^i + \Psi^j)\Phi_2 < 0,\ 1 \le i < j \le 2 \end{aligned} \tag{58}$$

where

$$\check{\Upsilon}^{ij} = \begin{bmatrix} \bar{\Upsilon}_{11}^{ij} & * & * & * \\ \bar{\Upsilon}_{21}^{ij} & \Upsilon_{22} & * & * \\ \bar{\Upsilon}_{31} & 0 & \Upsilon_{33} & * \\ \bar{\Upsilon}_{41} & 0 & 0 & \Upsilon_{44} \end{bmatrix} = \Phi_2^T \Upsilon^{ij} \Phi_2 \tag{59}$$

Applying Lemma 1 to $\Upsilon_{ii}(i = 2, 3, 4)$ in (59), we obtain $\bar{\Upsilon}_{ii}(i = 2, 3, 4)$ in (53). Thus, if satisfying the conditions in Theorem 2, the DC microgrid system (21) under the FDI attacks, the DETM, network delays and imperfect premise matching is mean-square exponentially stable, and gain matrices $K_j = Y_j X^{-1}$ of the current injection fuzzy controller (18) and the parameter $\Omega = X^{-1}\bar{\Omega}X^{-1}$ of the DETM (12) can be derived simultaneously.

Remark 6. Unlike the two-step emulation based method in [29] that a controller is first designed without considering the ETM, and then the ETM is designed to save communication resources while maintaining system stability, the co-design method in Theorem 2 can compute parameters of the injection current controller and the DETM simultaneously, which simplifies the whole design procedure.

Remark 7. Unlike existing work on the dynamic ETM [30], FDI attacks [31] or fuzzy control [19], this paper considers the effects of the dynamic ETM, FDI attacks, network delays, T-S fuzzy controller with premise mismatching and CPL-induced instability issue simultaneously all in one unified framework, which is more comprehensive and practical but quite challenging to find a feasible injection current controller based on the linear matrix inequalities given in Theorem 2. Fortunately, by using the reciprocally convex method [27] and the slack matrices $\Psi^i(i = 1, 2)$ in Theorem 1 to reduce conservativeness, Theorem 2 can generate the feasible controllers as shown in the following section.

5. Case studies

5.1. Example of a DC microgrid with one CPL

Table 1: Parameters for a DC microgrid with one CPL.

r_1	1.1 Ω	$x_{1,20}$	196.64 V	C_s	500 μF
L_1	39.5 mH	$\tilde{w}_{2,1}$	130.4 V	V_{dc}	200 V
C_1	500 μF	r_s	1.1 Ω		
P_1	300 W	L_s	39.5mH		

A benchmark DC microgrid system in [18] is introduced to verify the proposed method. The circuit parameters of the DC microgrid with one CPL are given in Table 1. Other parameters are given as: sampling period $h = 0.5ms$, delay bounds $\tau_m = 0.1ms, \tau_M = 0.2ms$, parameters of the DETM $\delta_1 = 0.006, \delta_0 = 0.004, \varrho = 50$, attack expectation $\bar{\alpha} = 0.15$, attack signal $\mathscr{F}(t) = -tanh(G\bar{x}(t))$ with $G = 0.3I$, scalars $\rho_1 = 0.9, \rho_2 = 0.8, \sigma = 1, \varepsilon_i = 0.0015(i = 1, \ldots, 5)$, and the initial condition $\tilde{x}_0 = [19 \ -30 \ 19 \ -30]^T$.

Using Theorem 2, parameters of the current injection fuzzy controller and the DETM can be simultaneously derived as

$$\begin{cases} K_1 = \begin{bmatrix} 1.1844 & 0.0641 & 0.3761 & 0.1698 \end{bmatrix} \\ K_2 = \begin{bmatrix} 1.1799 & 0.0678 & 0.3779 & 0.1699 \end{bmatrix} \end{cases} \tag{60}$$

$$\Omega = \begin{bmatrix} 10.8648 & 0.5552 & 1.7276 & 0.5802 \\ 0.5552 & 0.1552 & -0.0081 & 0.0302 \\ 1.7276 & -0.0081 & 3.0344 & 0.1297 \\ 0.5802 & 0.0302 & 0.1297 & 0.1034 \end{bmatrix} \tag{61}$$

As shown in Figure 5, the DC microgrid is unstable in open-loop operation, which is consistent with the Figure 3 in [20]. Considering the effects of the FDI attacks, the DETM, network delays and imperfect premise matching, the designed current injection fuzzy controller can drive both voltage and current responses of the DC microgrid to the equilibrium points, respectively. Specially, the data tips show that the capacitor voltage and inductor current of the CPL subsystem eventually converge to $196.64V$ and $1.5256A$, respectively, which are consistent with their corresponding state operating points $x_{1,20} = 196.64V$ (as shown in Table 1) and $x_{1,10} = P1/x_{1,20} = 1.5256A$.

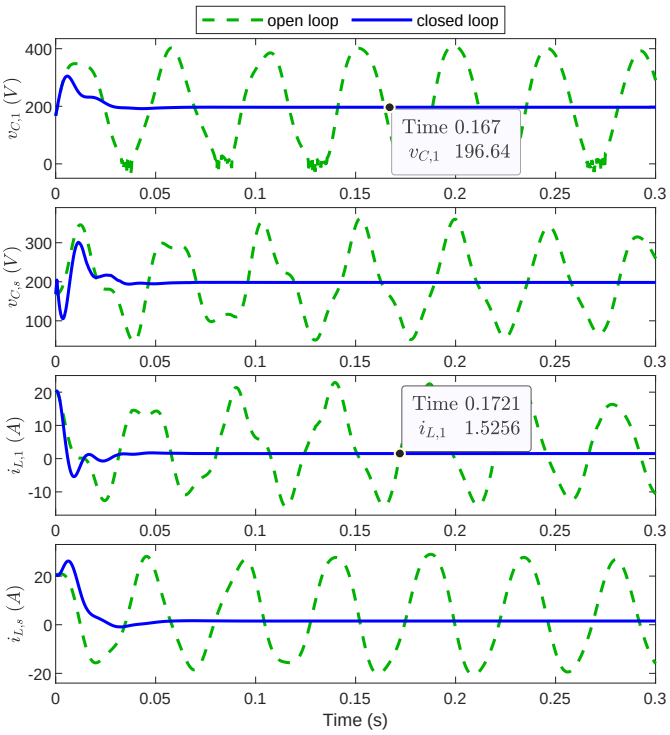

Figure 5: Voltage and current responses of the DC microgrid.

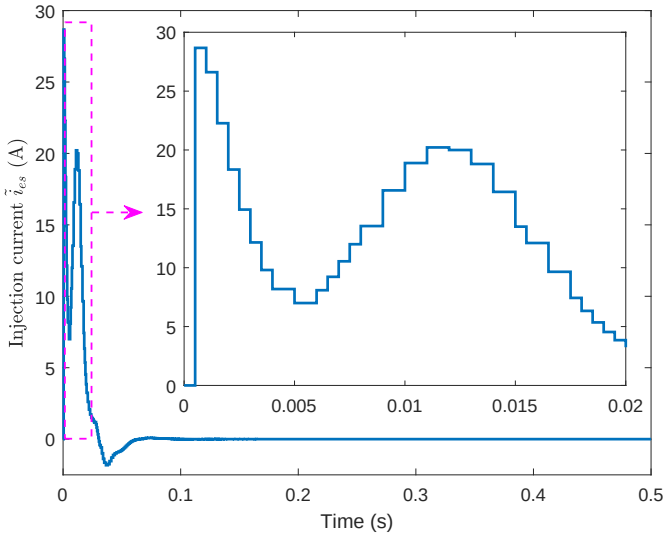

Figure 6: The injection current $\tilde{i}_{es}$.

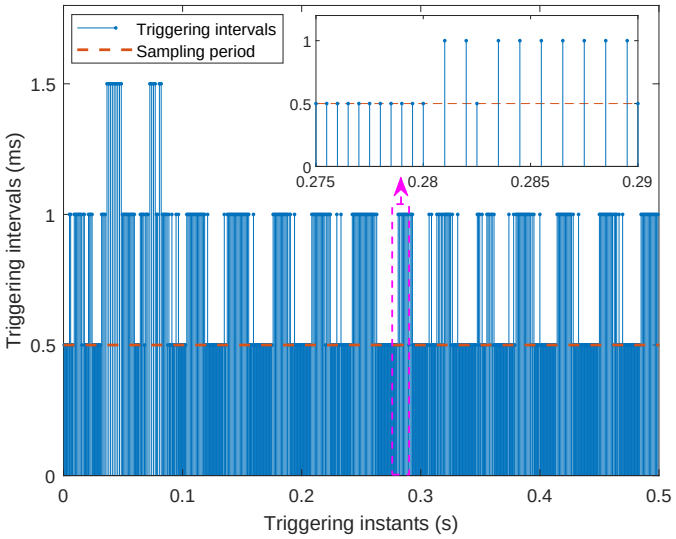

Figure 7: Triggering instants and triggering intervals of the DETM.

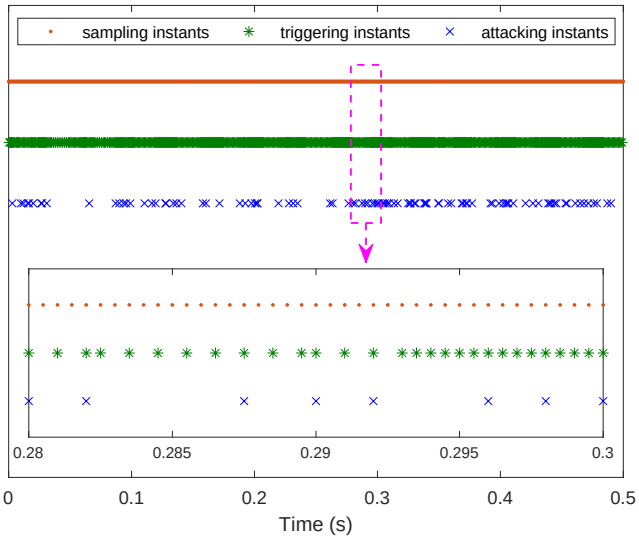

Figure 8: Attacking instants of the FDI attacks.

Figure 6 shows that the injection current $\tilde{i}_{es}$ eventually converges to zero. Namely, when the DC microgrid arrives at the equilibrium point, it is unnecessary to inject current from the ESS. Besides, the zoomed graph indicates that the injection current is piecewise constant during triggering intervals, since $\tilde{i}_{es}$ does not change until the controller receives a transmitted data from the DETM.

Figure 7 shows triggering intervals and triggering instants of the DETM. Many triggering intervals are larger than the sampling period $0.5ms$. The triggering rate of the DETM can be computed as $r_t = n_t/n_s = 72.5\%$, where $n_s = 1000$ and $n_t = 725$ denote the numbers of the sampled data and the transmitted data, respectively. Compared with the TTM transmitting all the sampled data (i.e., $r_t = 100\%$), the DETM can save 27.5% of communication resources. The zoomed graph shows that the minimum triggering interval $0.5ms$ equals to the sampling period, which confirms the Zeno-free property of the DETM in Remark 2.

Figure 8 shows sampling instants, triggering instants of the DETM and attacking instants of the FDI attacks. Among the 1000 sampling instants, only 725 of them satisfying the triggering condition become triggering instants. Among these 725 triggering instants, 98 of them are attacked by random FDI attacks, which implies the attacking rate is $r_a = 13.5\%$. The zoomed graph describes the relationship among sampling instants, triggering instants and attacking instants in detail.

In summary, considering effects of the FDI attacks, the DETM, network delays and imperfect premise matching, although only 72.5% of the sampled data are transmitted by the DETM, and 13.5% of the transmitted data are tampered by the FDI attacks, the designed current injection fuzzy controller can still obtain satisfactory control performance while the DETM saves 27.5% of communication bandwidth, which confirms the effectiveness of the proposed method.

5.2. Comparison with SETM [17] and DETM [30]

Considering the DC microgrid (39) without the FDI attacks, Corollary 1 is used to co-design the current injection controller and the DETM (12). As shown in Figure 9, the triggering threshold of the SETM [17] is smaller than that of the DETM (12), and thus, the transmitting rate 84.5% of the SETM is higher than 67.5% of the DETM, which confirms Remark 3. Besides, the state-error term $\|\Phi^{\frac{1}{2}}e(t)\|^2$ does not exceed the triggering threshold of the DETM (12), and it becomes zero at each triggering instant. Moreover,

although the DETM (12) consumes less communication resources, it still achieves competitive control performance with respect to the SETM [17] and the TTM.

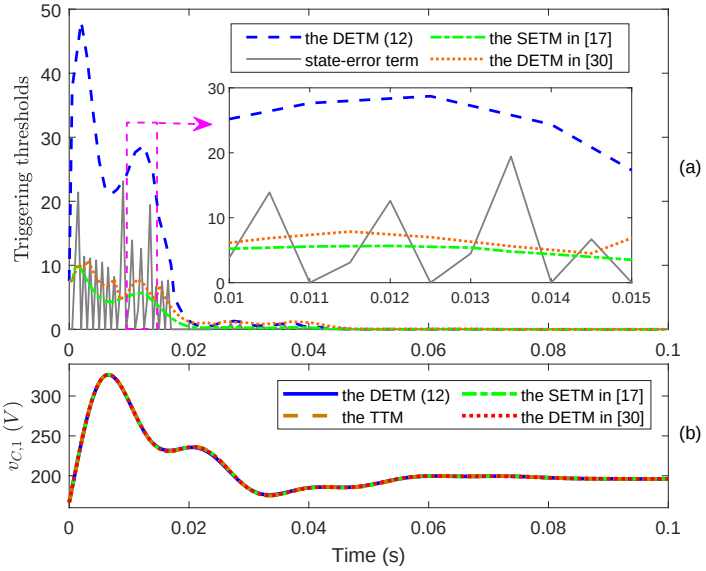

Figure 9: Comparisons among the SETM [17], the DETM [30] and the DETM (12) in: (a) triggering performance, and (b) control performance.

It should be noted that the work [30] presents another DETM with a triggering threshold parameter $\sigma(t) = \hat{\sigma} + (\bar{\sigma} - \hat{\sigma})e^{-\varrho\|\Phi^{0.5}e(t)\|^2}$. During the transient response, a large state error $\|e(t)\|$ results in a small $\sigma(t)$, and thus, as shown in Figure 9 (a), the triggering threshold of the DETM [30] is slightly larger than that of the SETM [17]. On the other hand, for the proposed DETM (12), a large state error $\|e(t)\|$ leads to a large dynamic threshold parameter $\delta_d(t) = \delta_1 tanh(\varrho\|e(t)\|)$, which provides a much larger triggering threshold than that of the DETM [30]. As shown in Figure 9 (b), the proposed controller under the DETM (12) in this paper not only consumes far less communication resources, but also achieves almost identical control performance as the method [30]. In other word, the proposed method achieves the similar control performance as the DETM [30] but consuming much less communication resources.

Figure 10 describes effects of parameters $\|e(t)\|, \delta_1$ and ϱ on the dynamic threshold parameter $\delta_d(t)$ of the DETM (12). Denoting $\bar{\delta}_d(t) = \delta_d(t)/max(\delta_d(t))$ and $\|\bar{e}(t)\| = \|e(t)\|/max(\|e(t)\|)$, Figure 10 (a) shows that

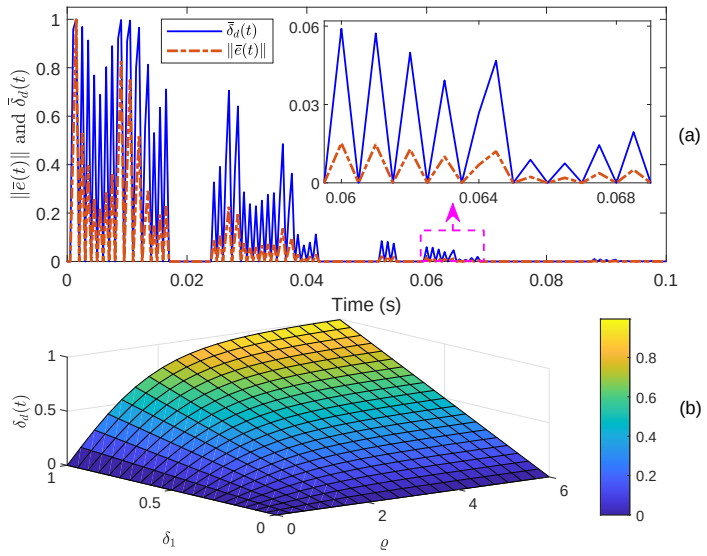

Figure 10: Effects of the triggering threshold parameters in the DETM

the normalized dynamic threshold parameter $\bar{\delta}_d(t)$ varies adaptively with the normalized state-error norm $\|\bar{e}(t)\|$, which helps the DETM save more communication resources during the transient response. Figure 10 (b) shows that, a larger threshold parameter δ_1 or ϱ leads to a larger dynamic threshold parameter $\delta_d(t)$, which helps the DETM reduce the triggering rate further.

5.3. Comparison with the robust linear controller [20]

To further verify the proposed methods, as shown in Figure 11 (a), a hardware-in-loop experiment platform is established, which consists of a micro-controller TMS320F28069M, real-time system simulator Typhoon HIL 604 and a host computer. As shown in Figure 11 (b), using the host computer, microgrid model and controller code are firstly embedded in Typhoon HIL 604 and TMS320F28069M through universal-serial-bus interfaces, respectively. Then, Typhoon HIL 604 and TMS320F28069M work as the microgrid and controller, respectively, and they communicate through a launchpad interface. Typhoon HIL 604 generates real-time microgrid states and sends them to TMS320F28069M for controller update. Meanwhile, TMS320F28069M computes control signals and controls the microgrid in Typhoon HIL 604.

Considering the microgrid system (43) without the FDI attacks and the DETM, and using the proposed Corollary 2 and the method in [20], the injec-

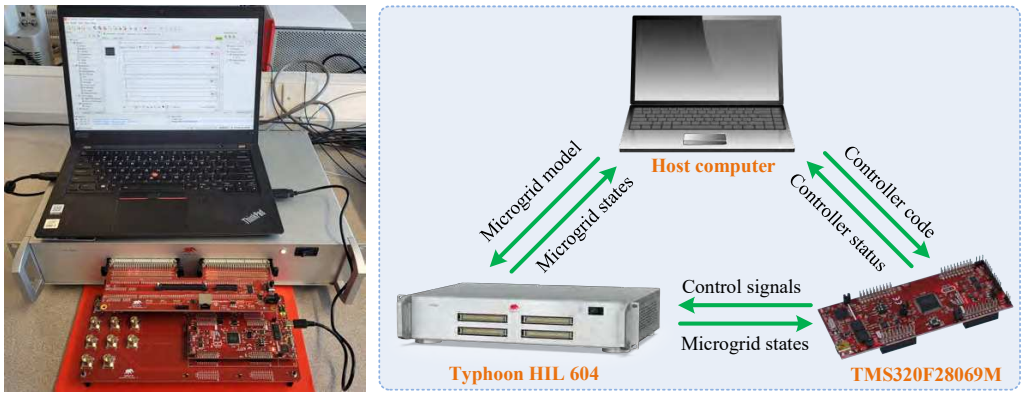

Figure 11: Microgrid experiment platform (a) and its structure (b).

tion current fuzzy controller and the robust linear controller are respectively obtained as

$$\text{T-S fuzzy controller: } \begin{cases} K_1 = \begin{bmatrix} 0.8581 & 0.0420 & 0.8502 & 0.1751 \end{bmatrix} \\ K_2 = \begin{bmatrix} 0.8562 & 0.0428 & 0.8508 & 0.1751 \end{bmatrix} \end{cases} \tag{62}$$

$$\text{Robust linear controller: } K = \begin{bmatrix} -1.0549 & -0.1585 & 0.9932 & 0.1958 \end{bmatrix} \tag{63}$$

As shown in Figure 12 and Table 2, the proposed T-S fuzzy controller (62) achieves the smaller maximum overshoot and faster convergence speed than the robust linear controller in [20], where the settling time refers to the time instant t_s satisfying $\|v_{C,1} - v_{C0,1}\| < v_{C0,1} \times 5\%, \forall t > t_s$. Namely, the T-S fuzzy control strategy is more effective in handling the CPL-induced nonlinear issues, which confirms Remark 1. When considering effects of the DETM and FDI attacks, the ETFSIC controller (60) obtains the similar performance as the T-S fuzzy controller but with a slower convergence speed. However, the ETFSIC controller consumes 42.67% less communication resources than the T-S fuzzy controller. Namely, the ETFSIC controller can make tradeoffs between control and communication performances.

Remark 8. The control objective in this study is set to drive the unstable DC microgrid to the equilibrium point by designing an ETFSIC controller, while considering effects of the FDI attacks, the dynamic ETM, network delays, premise mismatching and CPL-induced instability issue simultaneously. Both simulation and experimental results show that the ETFSIC controller

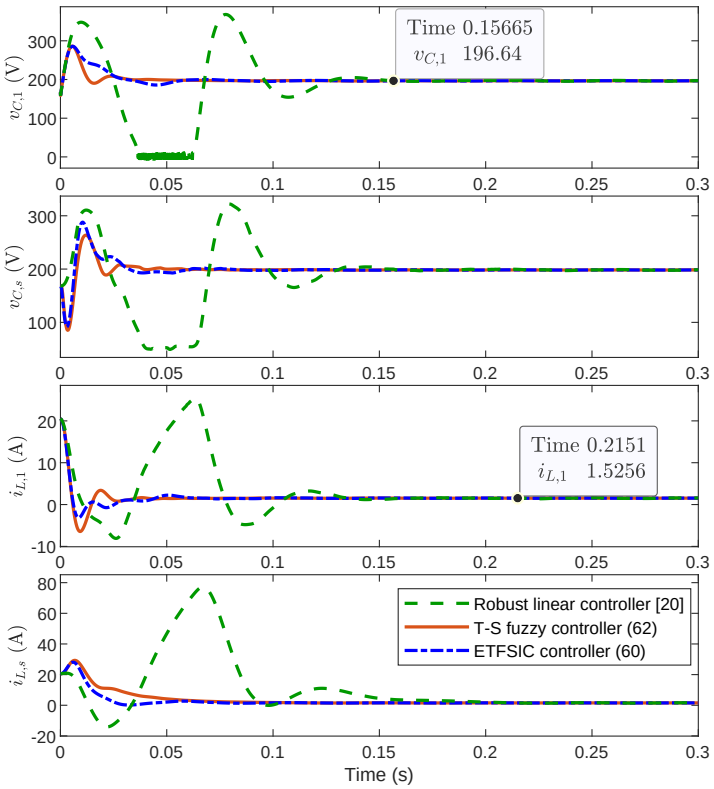

Figure 12: Microgrid states under the T-S fuzzy controller (62), the ETFSIC controller (60) and robust linear controller [20].

Table 2: Maximum overshoot and settling time

Methods	Maximum overshoot (%)				Settling time (ms)			
	$v_{C,1}$	$v_{C,s}$	$i_{L,1}$	$i_{L,s}$	$v_{C,1}$	$v_{C,s}$	$i_{L,1}$	$i_{L,s}$
Robust linear controller [20]	87.17	62.36	1570	4959	122	123	254	320
T-S fuzzy controller (62)	45.54	32.91	122.8	1820	26.6	18.4	53.3	112
ETFSIC controller (60)	45.34	45.18	47.40	1740	47.6	29.1	107	158

can stabilise the DC microgrid (as shown in Figure 5), and it performs better than the robust linear controller in [20] in terms of overshoot and settling time (as shown in Figure 12 and Table 2). Some other advanced control strategies such as the memory-based dynamic event-triggered control method [32] will also be investigated in the microgrid control as a future work.

6. Conclusions

The paper studies the dynamic event-triggered fuzzy control of DC microgrids with FDI attacks and imperfect premise matching. First, due to the inclusion of the adaptive triggering threshold parameter, the proposed DETM can save more communication resources than the SETM, and it is Zeno-free due to its discrete time feature. Then, taking effects of the FDI attacks, the DETM, network delays and imperfect premise matching into account, a unified T-S fuzzy closed loop system model is built for DC microgrids. Next, using Lyapunov theory, sufficient conditions for the mean-square exponential stability are achieved, which shed a light on how the factors affect the system performance. Further, a co-design method of the current injection fuzzy controller and the DETM is presented such that tradeoffs between control and communication performances can be made in a unified framework, which is more convenient than the emulation based method.

Finally, case studies confirm the effectiveness of the proposed method. To stabilize the DC microgrid with one CPL, the DETM only transmits 72.5% of the sampled data, which implies 27.5% of communication resources can be saved. Particularly, even 13.5% of the transmitted data are tampered by the FDI attacks, the designed current injection fuzzy controller still works well in stabilizing the DC microgrid. Comparisons show that while achieving similar control performances, the transmitting rate of the DETM is 67.5%, which is lower than 84.5% of the SETM. Besides, due to the nonlinear feature of the CPLs in DC microgrids, the proposed T-S fuzzy controller performs better than the robust linear controller.

CRediT authorship contribution statement

Fuqiang Li: Conceptualization, Validation, Methodology, Writing-Original draft. Kang Li: Supervision, Conceptualization, Writing-Review and Editing. Chen Peng: Methodology, Supervision, Writing-Review and Editing. Lisai Gao: Methodology, Data Curation, Software.

Declaration of competing interest

The authors declare that they have no known competing financial interests or personal relationships that could have appeared to influence the work reported in this paper.

Acknowledgments

This work was supported by National Natural Science Foundation of China [grant no. 61703146]; Scientific Project in Henan Province [grant no. 202102110126]; Backbone Teacher in Henan Province [grant no. 2020GGJS048].

References

[1] Z. Zhang, O. Babayomi, T. Dragicevic, R. Heydari, C. Garcia, J. Rodriguez, R. Kennel, Advances and opportunities in the model predictive control of microgrids: Part I-primary layer, International Journal of Electrical Power and Energy Systems 134 (2022) 107411.

[2] Y. Yang, J. Xu, Q. Wu, C. Li, W. Zhang, An impedance amplitude compensation control strategy for improvement of dynamic performance of DC microgrid, International Journal of Electrical Power and Energy Systems 136 (2022) 107462.

[3] J. Li, H. Pan, X. Long, B. Liu, Objective holographic feedbacks linearization control for boost converter with constant power load, International Journal of Electrical Power and Energy Systems 134 (2022) 107310.

[4] Q. Xu, N. Vafamand, L. Chen, T. Dragievi, L. Xie, F. Blaabjerg, Review on advanced control technologies for bidirectional DC/DC converters in DC microgrids, IEEE Journal of Emerging and Selected Topics in Power Electronics 9 (2) (2021) 1205–1221.

[5] S. Hu, D. Yue, C. Dou, X. Xie, Y. Ma, L. Ding, Attack-resilient event-triggered fuzzy interval type-2 filter design for networked nonlinear systems under sporadic denial-of-service jamming attacks, IEEE Transactions on Fuzzy Systems 30 (1) (2022) 190–204.

[6] Y. Pan, Y. Wu, H.-K. Lam, Security-based fuzzy control for nonlinear networked control systems with DoS attacks via a resilient event-triggered scheme, IEEE Transactions on Fuzzy Systems 30 (10) (2022) 4359–4368.

[7] S. Madichetty, S. Mishra, Cyber attack detection and correction mechanisms in a distributed DC microgrid, IEEE Transactions on Power Electronics 37 (2) (2022) 1476 – 1485.

[8] M. R. Habibi, H. R. Baghaee, F. Blaabjerg, T. Dragievi, Secure MPC/ANN-based false data injection cyber-attack detection and mitigation in DC microgrids, IEEE Systems Journal 16 (1) (2022) 1487–1498.

[9] A. Cecilia, S. Sahoo, T. Dragievi, R. Costa-Castell, F. Blaabjerg, On addressing the security and stability issues due to false data injection attacks in DC microgridsan adaptive observer approach, IEEE Transactions on Power Electronics 37 (3) (2022) 2801–2814.

[10] J. Zhou, Q. Yang, X. Chen, Y. Chen, J. Wen, Resilient distributed control against destabilization attacks in DC microgrids, IEEE Transactions on Power Systems 37 (2022) 1–14.

[11] Y. Jiang, Y. Yang, S.-C. Tan, S. Y. Hui, Distributed sliding mode observer-based secondary control for DC microgrids under cyber-attacks, IEEE Journal on Emerging and Selected Topics in Circuits and Systems 11 (1) (2021) 144–154.

[12] C. Peng, J. Wu, E. Tian, Stochastic event-triggered H_∞ control for networked systems under denial of service attacks, IEEE Transactions on Systems, Man, and Cybernetics: Systems 52 (7) (2022) 4200–4210.

[13] Z. Chen, X. Yu, W. Xu, G. Wen, Modeling and control of islanded DC microgrid clusters with hierarchical event-triggered consensus algorithm, IEEE Transactions on Circuits and Systems I: Regular Papers 68 (1) (2021) 376–386.

[14] J. Peng, B. Fan, Q. Yang, W. Liu, Distributed event-triggered control of DC microgrids, IEEE Systems Journal 15 (2) (2021) 2504–2514.

[15] L. Xing, Q. Xu, F. Guo, Z.-G. Wu, M. Liu, Distributed secondary control for DC microgrid with event-triggered signal transmissions, IEEE Transactions on Sustainable Energy 12 (3) (2021) 1801–1810.

[16] P. Shafiee, Y. Khayat, Y. Batmani, Q. Shafiee, J. M. Guerrero, On the design of event-triggered consensus-based secondary control of DC microgrids, IEEE Transactions on Power Systems 37 (5) (2022) 3834–3846.

[17] J. Zhang, H. Zhang, A high-reliability event-triggered secondary control strategy for microgrid considering time-varying delay, IEEE Systems Journal 16 (2022) 1–12.

[18] M. M. Mardani, N. Vafamand, M. H. Khooban, T. Dragievi, F. Blaabjerg, Design of quadratic D-Stable fuzzy controller for DC microgrids with multiple CPLs, IEEE Transactions on Industrial Electronics 66 (6) (2019) 4805–4812.

[19] N. Vafamand, M. H. Khooban, T. Dragicevic, F. Blaabjerg, J. Boudjadar, Robust non-fragile fuzzy control of uncertain DC microgrids feeding constant power loads, IEEE Transactions on Power Electronics 34 (11) (2019) 11300–11308.

[20] L. Herrera, W. Zhang, J. Wang, Stability analysis and controller design of DC microgrids with constant power loads, IEEE Transactions on Smart Grid 8 (2) (2017) 881 – 888.

[21] H. Liang, L. Chen, Y. Pan, H.-K. Lam, Fuzzy-based robust precision consensus tracking for uncertain networked systems with cooperative-antagonistic interactions, IEEE Transactions on Fuzzy Systems 30 (2022) 1–15.

[22] X. Chen, C. Hu, E. Tian, C. Peng, Event-based fuzzy resilient control of nonlinear DC microgrids under denial-of-service attacks, ISA Transactions 127 (2022) 206–215.

[23] C. Peng, F. Li, A survey on recent advances in event-triggered communication and control, Information Sciences 457-458 (2018) 113 – 125.

[24] J. Liu, Y. Wang, L. Zha, X. Xie, E. Tian, An event-triggered approach to security control for networked systems using hybrid attack model,

International Journal of Robust and Nonlinear Control 31 (12) (2021) 5796 – 5812.

[25] E. Tian, C. Peng, Memory-based event-triggering H_∞ load frequency control for power systems under deception attacks, IEEE Transactions on Cybernetics 50 (11) (2020) 4610–4618.

[26] L. Zou, Z. Wang, Q.-L. Han, D. Zhou, Ultimate boundedness control for networked systems with try-once-discard protocol and uniform quantization effects, IEEE Transactions on Automatic Control 62 (12) (2017) 6582–6588.

[27] P. Park, J. W. Ko, C. Jeong, Reciprocally convex approach to stability of systems with time-varying delays, Automatica 47 (1) (2011) 235 – 238.

[28] Z. Gu, X. Sun, H.-K. Lam, D. Yue, X. Xie, Event-based secure control of T-S fuzzy-based 5-DOF active semivehicle suspension systems subject to DoS attacks, IEEE Transactions on Fuzzy Systems 30 (6) (2022) 2032–2043.

[29] W. Wang, R. Postoyan, D. Nesic, W. Heemels, Periodic event-triggered control for nonlinear networked control systems, IEEE Transactions on Automatic Control 65 (2) (2020) 620 – 635.

[30] I. Ahmad, X. Ge, Q.-L. Han, Decentralized dynamic event-triggered communication and active suspension control of in-wheel motor driven electric vehicles with dynamic damping, IEEE/CAA Journal of Automatica Sinica 8 (5) (2021) 971–986.

[31] G. Cao, W. Gu, G. Lou, W. Sheng, K. Liu, Distributed synchronous detection for false data injection attack in cyber-physical microgrids, International Journal of Electrical Power and Energy Systems 137 (2022) 107788.

[32] X. Li, D. Ye, Memory-based dynamic event-triggered control for networked interval type-2 fuzzy systems subject to DoS attacks, International Journal of Adaptive Control and Signal Processing 36 (1) (2022) 104 – 121.